Catalysis Today 143 (2009) 80–85

Contents lists available at ScienceDirect

Catalysis Today

journal homepage: www.elsevier.com/locate/cattod

Basic evidences for methanol-synthesis catalyst design

F. Arena [a,b], G. Italiano [a], K. Barbera [c], G. Bonura [b], L. Spadaro [b], F. Frusteri [b,*]

[a] Dipartimento di Chimica Industriale e Ingegneria dei Materiali, Università degli Studi di Messina, Salita Sperone 31 c.p. 29, I-98166 S. Agata (Messina), Italy
[b] Istituto CNR-ITAE "Nicola Giordano", Salita S. Lucia 5, I-98126 S. Lucia (Messina), Italy
[c] Dipartimento di Chimica Inorganica, Fisica e dei Materiali, NIS Centre of Excellence and Centro di Riferimento INSTM, University of Turin, Via P. Giuria 7, I-10125 Torino, Italy

ARTICLE INFO

Article history:
Available online 8 January 2009

Keywords:
$Cu–ZnO/ZrO_2$ catalysts
Solid-state interactions
Adsorption properties
Surface sites
Dispersion
Oxide/metal interface
Catalytic functionality
CO_2-hydrogenation
Methanol

ABSTRACT

A series of $Cu–ZnO/ZrO_2$ catalysts (Zn_{at}/Cu_{at}, 0–3; ZrO_2, 42–44 wt.%) with markedly improved total (SA, 120–180 m^2/g) and metal surface area (MSA, 9–63 m^2/g) has been synthesized via the *reverse co-precipitation under ultrasound field*. Structure, adsorption properties and surface reactivity were probed by BET, XRD, TPR, N_2O-titration and TPD measurements of H_2, CO and CO_2, while the activity pattern in the CO_2 to CH_3OH hydrogenation reaction (T_R, 433–473 K; P_R, 1.0 MPa) has been addressed. An optimum ZnO loading (Zn_{at}/Cu_{at}, 0.3–0.8) ensures higher process productivity, while the apparent *structure sensitive* character of the title reaction relies on the synergism of *metal hydrogenation* and *oxide basic* sites (*dual-site*). The extent of the oxide/metal interface, probed by $Cu^{\delta+}/Cu^0$ and oxide-to-metal surface area (OSA/MSA) ratios, is the key-parameter allowing the normalization of the catalytic specific activity in a wide range (3–60%) of metal dispersion and the consequent *structure insensitive* character of the CO_2 hydrogenation reaction.

1. Introduction

Among the various available strategies to reduce carbon dioxide emissions, novel process technologies for CO_2-recycling are currently attracting a great scientific and technological concern [1–4]. In particular, the use of CO_2 as "reagent" for producing bulk chemicals and fuels like methanol (MeOH) and dimethyl ether (DME) [1–5] looks very attractive since, as alternatives to gasoline and gasoil, they ensure superior combustion efficiency and much lower air pollution than oil-based fuels [1,2]. Nowadays the industrial synthesis of methanol is carried out at 493–573 K and 5–10 MPa pressure by feeding a $CO(5\%)–CO_2(5\%)–H_2$ syngas stream on $Cu–ZnO/Al_2O_3$ catalysts [6–9]. Under such conditions methanol mostly forms from CO_2 with CO acting as "tuner" of the WGS equilibrium reaction and *scavenger* of oxygen atoms from the catalyst surface [6–9]. However, an effective CO_2 conversion is at present limited by a poor specific functionality of current catalysts [10,11], likely due to the strong *hydrophilic* character of alumina carrier, and perhaps ZnO, involving a marked negative effect of water on active sites stability [17–22]. Then, Cu/ZrO_2 and $Cu–ZnO/ZrO_2$ systems ensure a superior CO_2 hydrogenation functionality in comparison to conventional catalysts [12–17], though solid-state interactions and reaction atmosphere influence the extent of the metal/oxide interface, playing a crucial influence on the catalytic functionality of Cu systems [17–21].

Therefore, this paper deals with a systematic investigation of the effects of the Zn/Cu ratio on the structure and adsorption properties of the $Cu–ZnO/ZrO_2$ system to shed light into its reactivity pattern in the CO_2-to-methanol hydrogenation reaction [22,23].

2. Experimental

A series of $Cu–ZnO/ZrO_2$ catalysts with a constant zirconia loading (41–44 wt.%) and Zn_{at}/Cu_{at} atomic ratio between 0 and 2.8 was prepared via the *reverse co-precipitation under ultrasound field* [22,23]. After washing the catalysts were dried at 373 K and further calcined in air at 623 K (4 h). The list of catalysts with the relative notation and main physico-chemical properties is given in Table 1.

Surface area (SA) and pore volume (PV) values of "as prepared" catalysts were determined from nitrogen adsorption–desorption isotherms at 77 K, using an ASAP 2010 (*Micromeritics Instrument*) gas adsorption device. The isotherms were elaborated by BET method for SA calculation, while Horwarth–Kavazoe and BJH methods were used for micro and mesopores evaluation, respectively [22,23].

X-ray diffraction (XRD) analysis in the 2θ range 10–70° was performed using a *Philips X-Pert* diffractometer operating with Ni β-filtered Cu Kα radiation at 40 kV and 30 mA and a scan step of 0.05°/min.

* Corresponding author. Tel.: +39 090624233.
E-mail address: francesco.frusteri@itae.cnr.it (F. Frusteri).

0920-5861/$ – see front matter © 2008 Published by Elsevier B.V.
doi:10.1016/j.cattod.2008.11.022

Table 1
List of the studied catalysts and relative physico-chemical properties.

Code	Chemical composition (wt.%)			Zn_{at}/Cu_{at}	SA_{BET} (m^2/g_{cat})	P.V. (cm^3/g_{cat})	A.P.D. (Å)	MSA[a] (m^2_{Cu}/g_{cat})	D_{Cu}[a] (%)	d_{Cu}[a] (nm)
	CuO	ZnO	ZrO_2							
CZ	58.6	0	41.4	0	118	0.25	74	8.7	3.3	31.5
10ZCZ	51.9	4.6	43.5	0.1	128	0.24	91	17.4	6.2	16.8
40ZCZ	41.2	14.8	44.0	0.4	174	0.56	106	60.8	29.1	3.6
80ZCZ	31.6	24.0	44.4	0.8	159	0.36	85	59.3	37.0	2.8
280ZCZ	15.1	41.8	43.1	2.8	147	0.35	73	44.7	57.9	1.8
ZZ	0	56.1	43.9	–	103	0.31	121	–	–	–

[a] From "single-pulse" (1.0 mL) N_2O titration measurements at 363 K.

Metal dispersion (D) values were obtained by "single-pulse" N_2O titration measurements [22,23]. Before measurements the samples were reduced at 573 K in flowing H_2 (1 h), then "flushed" at 583 K in the N_2 carrier flow (15 min) and further cooled down. Henceforth this is referred as the *standard activation treatment*, (e.g., "pre-reduction"). Dispersion and metal surface area (MSA) were calculated assuming a $Cu:N_2O = 2$ titration stoichiometry and a surface atomic density of 1.46×10^{19} Cu_{at}/m^2, respectively [22,23].

Temperature programmed reduction (TPR) measurements in the range 273–1073 K of the "as prepared" (AP), "pre-reduced" (PR) and further "CO_2-treated" *in situ* (PR/CO_2) (T_R, 473 K; treatment mixture, 10%CO_2/He; flow rate, 100 stp mL/min; exposure time, 1 h) catalyst samples (≈15 mg) were performed in a continuous flow apparatus using a quartz micro-reactor fed with a 6%H_2/Ar mixture flowing at 60 stp mL/min and heated at rate of 20 K/min.

TPD measurements of H_2 (H_2-TPD) were carried out in the range 293–773 K with a heating rate of 20 K/min using Ar as carrier gas (30 stp mL/min). After the standard activation treatment, the samples were cooled to r.t. and further saturated in H_2 for 15 min, then flushed by the carrier flow until stabilization of the baseline. The desorption process was monitored by a TCD quantitatively calibrated by H_2 pulses.

TPD measurements of CO (CO-TPD) and CO_2 (CO_2-TPD) were carried out with a heating rate of 20 K/min using He as carrier gas (30 stp mL/min). Pre-reduced catalysts were cooled to r.t. and further saturated in either CO or CO_2 flow for 30 min. The CO (m/z, 28) and CO_2 (m/z, 44) desorption processes were monitored by a Quadrupole mass spectrometer following the mass-to-charge signals (m/z) 4, 28 and 44 relative to He, CO and CO_2, respectively. CO and CO_2 peak area was quantitatively calibrated by CO and CO_2 pulses.

Catalyst testing in the hydrogenation of CO_2 was performed in the range of 433–473 K, using an Inconel micro-reactor (i.d., 6 mm) operating at 1.0 MPa. A CO_2–H_2–N_2 reaction mixture in the molar ratio equal to 3/9/1 was fed at the rate of 80 stp mL/min on a 0.5 g catalyst sample diluted with 0.5 g of same-sized SiC (GHSV, 8800 NL h^{-1} kg_{cat}^{-1}). Prior to each test, the catalysts were reduced *in situ* at 573 K for 1 h in H_2 flow at atmospheric pressure. The reaction stream was analysed by a GC equipped with a two-column system connected to FID (CH_3OH, CH_3OCH_3) and TCD (CO, N_2, CO_2, H_2), respectively.

3. Results and discussion

3.1. Influence of carrier and promoter on the structure and reactivity of the metal Cu phase

Despite of the large amount of studies devoted during last decades to reaction mechanism, kinetics and catalyst optimization, the role of the various surface sites on methanol synthesis functionality is still undefined ([22,23] *and references therein*). This depends upon the great sensitivity of the surface composition and morphology to reaction atmosphere [24] hindering a full understanding of the Cu–Zn(O) functionality [22,23]. This prompted us to carry out a systematic investigation of the effects of carrier and promoter on structure and surface reactivity of the Cu–ZnO/ZrO_2 system for addressing basic structure–activity relationships.

The XRD patterns before (Fig. 1A) and after the standard reduction treatment (Fig. 1B) disclose a marked influence of Zn_{at}/Cu_{at} on catalyst structure that, in turn, is crucial for dispersion (Table 1) and reactivity of the Cu phase. Featureless patterns in Fig. 1A signal the lack of "long-range" crystalline order on promoted catalysts, while the occurrence of sharp reflection peaks at 35.6° and 38.8° are diagnostic of the presence of *tenorite* [JCPDS 5–661] at low ZnO loadings (i.e., $Zn_{at}/Cu_{at} \leq 0.1$). A very intimate mixing of nanosized oxide domains, hindering the formation of "ordered" crystalline phases, gives rise to Cu nanoparticles (1.8–3.6 nm) on catalysts with $Zn_{at}/Cu_{at} > 0.1$ (Table 1), while the

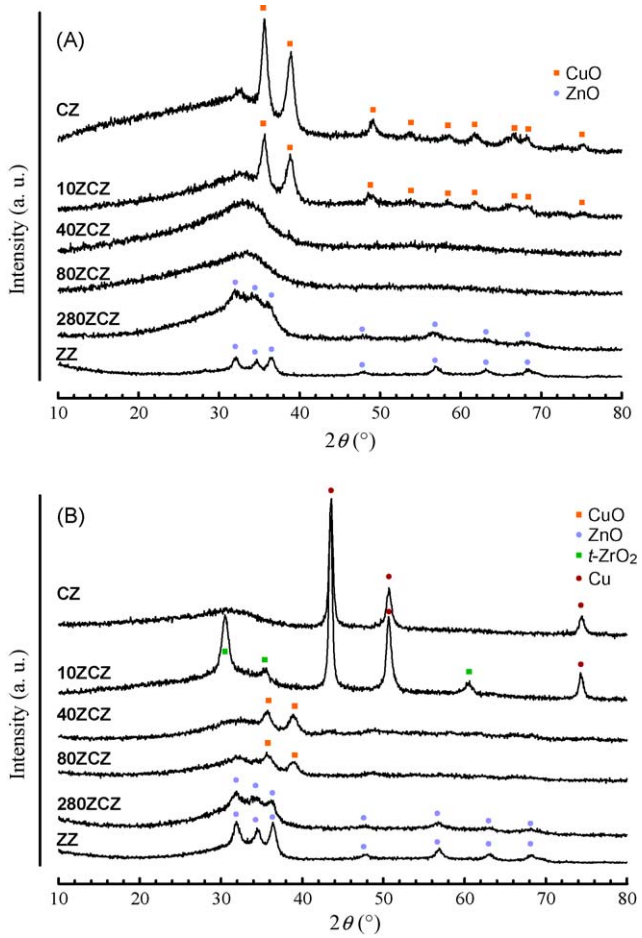

Fig. 1. XRD patterns of the "as prepared" (A) and "pre-reduced and air exposed" (B) samples of the studied catalysts.

presence of "large" crystalline CuO clusters accounts for the much poorer dispersion of CZ and 10ZCZ samples containing very small amounts, if any, of the ZnO promoter (Table 1). The promoting effect of ZnO on Cu dispersion and the concomitant decrease in Cu loading allow for the maximum MSA (ca. 60 m_{Cu}^2/g_{cat}) at intermediate (0.4–0.8) Zn_{at}/Cu_{at} values (Table 1).

The diffractograms of the passivated samples after the standard activation treatment show that the morphological features strongly affect the affinity of the metal phase to oxygen. The CZ and 10ZCZ samples present sharp reflections at 43°, 51° and 74° of the <1 1 1>, <2 0 0> and <2 1 1> facets of metal Cu [23], that are fully absent at higher Zn_{at}/Cu_{at}. Namely, the 40ZCZ and 80ZCZ catalysts display small lines of the *tenorite* phase, while those of *zincite* prevail on the 280ZCZ and ZZ samples. A poor metal dispersion and minor changes in the structure of the zirconia carrier further to reduction of the CZ and 10ZCZ samples denote on the whole a weak CuO–ZrO_2 interaction, while a much higher affinity between CuO and promoter emerges from the incipient crystallization of ZnO at higher Zn_{at}/Cu_{at} ratios. Evidently, ZnO acts as a "spacer" of nanosized Cu particles explaining the rise in dispersion with Zn_{at}/Cu_{at} [22,23]. Just the high dispersion favours an easy re-oxidation of promoted catalysts, at variance of CZ and 10ZCZ samples featuring a much lower reactivity to oxygen due to the large size of metal particles (Fig. 1B).

The affinity to CO_2 of the pre-reduced 10CZ, 40ZCZ and 280ZCZ catalysts was probed by the TPR analysis of pre-reduced (PR) and further CO_2 exposed samples at 473 K (PR/CO_2), shown in Fig. 2. The lack of any reduction peak below 673 K in the TPR profile of the *in situ* pre-reduced catalysts confirms the complete CuO reduction further to the standard activation treatment [23]. The subsequent CO_2 treatment (PR/CO_2) imply the appearance of a small peak in the spectra of the PR/CO_2 samples, indicating an incipient surface re-oxidation (6–18%) of the metal phase by CO_2, irrespective of the metal dispersion.

3.2. Adsorption properties and surface sites

A systematic study of the effects of Zn_{at}/Cu_{at} on type and abundance of surface adsorption sites has been performed by TPD measurements of molecules involved in methanol synthesis reactions (e.g., H_2, CO and CO_2). The various desorption profiles of H_2 (A), CO_2 (B) and CO (C) are shown in Fig. 3, while the maximum desorption temperature and quantitative data of H_2, CO_2 and CO desorption are summarized in Table 2.

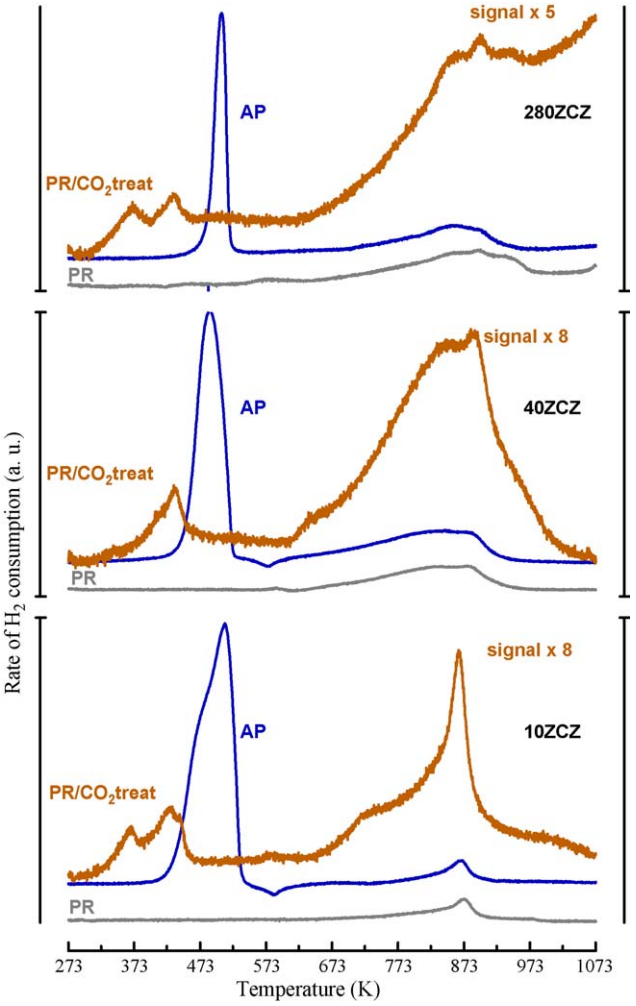

Fig. 2. TPR profiles of the "as prepared" (AP), "pre-reduced" (P_R), and "pre-reduced and CO_2 treated at 473 K" (P_R/CO_2 treat) samples of 10ZCZ, 40ZCZ and 280ZCZ catalysts.

Apart from the ZnO/ZrO_2 system, showing no affinity to hydrogen and CO, the H_2-TPD profiles of Cu/ZrO_2 and Cu–ZnO/ZrO_2 catalysts (Fig. 3A) are diagnostic of different hydrogen adsorption sites located at the surface and in the bulk of metal Cu

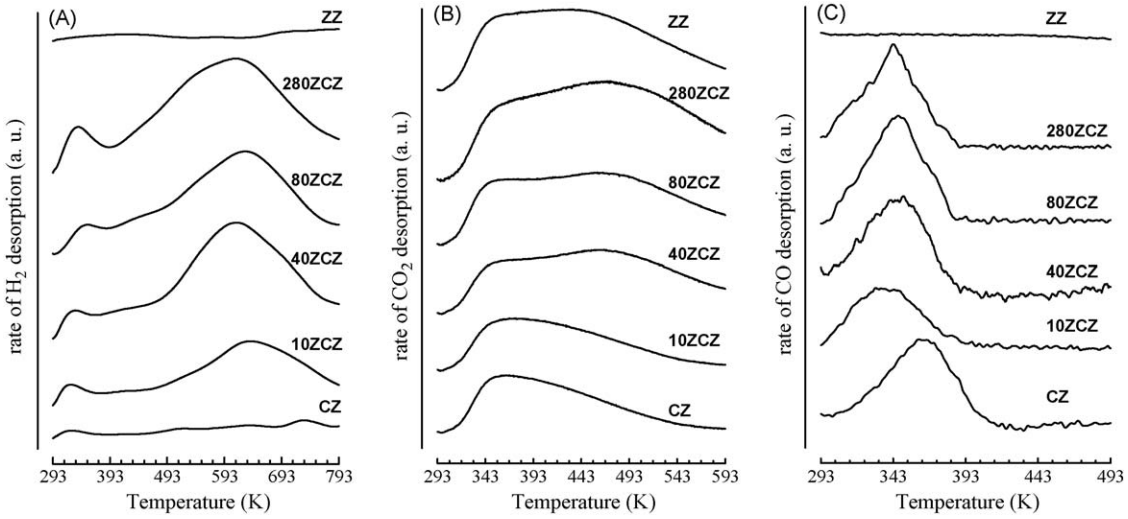

Fig. 3. H_2-TPD (A), CO_2-TPD (B) and CO-TPD (C) profiles of the various catalysts.

Table 2
H_2, CO and CO_2-TPD data. Desorption maximum temperature (T_{D1}) and amount desorbed.

Catalyst	T_{D1} (K)	T_{D2} (K)	H_2 desorption ($\mu mol/g_{cat}$) ($\mu mol/m_{Cu^2}$)[a]		H_2/N_2O	T_{CO} (K)	CO desorption ($\mu mol/g_{cat}$) ($\mu mol/m_{Cu^2}$)[b]		CO/N_2O	T_{CO_2} (K)	CO_2 desorption ($\mu mol/g_{cat}$)[b]	CO_2/SA ($\mu mol/m_{Cu^2}$)
CZ	327	739	91	8.8	0.16	361	7 (7)[c]	0.80	0.07	366	47	0.40
10ZCZ	328	635	211	12.2	1.00	331	5	0.29	0.02	378	44	0.34
40ZCZ	344	625	329	5.4	0.44	350	7 (4)[c]	0.12	0.01	467	68	0.39
80ZCZ	357	632	320	5.4	0.44	346	7	0.12	0.01	465	83	0.52
280ZCZ	344	630	363	8.2	0.67	343	6	0.13	0.01	467	111	0.76
ZZ	–	–	–	–	–	–	–	–	–	433	93	0.90

[a] In the range 293–773 K.
[b] In the range 293–573 K.
[c] Figures in parentheses refer to the amount of CO desorbed after the N_2O titration treatment.

and on surface ZnO sites [23,25–28]. Though increasing with the Zn_{at}/Cu_{at} ratio, the amount of H_2 follows a decreasing trend with the MSA exposure (Table 2). On the other hand, the CO_2-TPD profiles (Fig. 3B) disclose the presence of surface basic sites on all the studied systems irrespective of composition (Table 2). This relies on the fact that zirconia possesses its own surface Lewis basic sites, while the alkaline character of the ZnO promoter enhances the CO_2 affinity of the system [23]. Indeed, the CO_2-TPD pattern of CZ and 10ZCZ systems features a desorption maximum at ca. 360 K, markedly tailed on the high temperature side, that is characteristic of the basic sites of the zirconia carrier [17,23]. While, the broad component centred at 460–480 K signals the presence of strong basic sites associated with the promoter on catalysts with $Zn_{at}/Cu_{at} > 0.1$ (Table 2). The increasing ZnO loading results in a maximum CO_2 coverage on the ZZ sample (Table 2).

Then, to attain quantitative data on the effects of Zn_{at}/Cu_{at} and Cu dispersion on the surface affinity to CO, a systematic series of TPD measurements was performed (Fig. 3C). These data show only for the ZZ sample the lack of any surface affinity to CO, while all the other systems feature a similar desorption peak centred at 340–360 K, accounting for a concentration (6–7 $\mu mol/g_{cat}$) of CO adsorbing sites that corresponds to a minor fraction (CO/N_2O, 1–7%) of the surface exposed Cu atoms (Table 2). Considering the reversibility of CO adsorption on metal Cu atoms, quantitative CO-TPD data can be taken as a measure of the concentration of *electron-deficient* (i.e., $Cu^{\delta+}$) metal centres at metal-oxide(s) interface [23]. This is confirmed by supplementary CO-TPD measurements on the representative CZ and 40ZCZ catalysts subjected to the N_2O titration. Despite of similar spectral features, the CO uptake of the "N_2O-titrated" 40ZCZ sample is lower by ca. 50% than that of the reduced sample, while that of the CZ system remained substantially unchanged (Table 2). This suggests that a fraction of CO-adsorbing sites into ZnO-promoted systems is fairly sensitive to re-oxidation by N_2O [23]. According to the above structural characterization findings, these data signal that electron-deficient Cu sites in interaction with ZnO moieties (i.e., Cu–O–Zn) [24] are poorly resistant to oxidation at variance of $Cu^{\delta+}$ centres at the Cu–ZrO_2 interface [23]. Such a low stability of $Cu^{\delta+}$ sites looks as an indirect evidence of the poor stability of the Cu–ZnO interface that is likely at the origin of the worse CO_2-hydrogenation functionality of conventional catalysts in comparison to ZrO_2-supported ones [22]. Monitoring the concentration $Cu^{\delta+}$ and Cu^0 sites, respectively, henceforth the CO/N_2O ratio is taken as a measure of the extent of the oxide/metal interface [23].

3.3. Catalytic activity

Activity data of representative catalysts in the CO_2 hydrogenation reaction (GHSV, 8800 NL h^{-1} kg_{cat}^{-1}; P_R, 1.0 MPa) are summarized in Table 3 in terms of CO_2 conversion (X_{CO_2}) and CH_3OH selectivity (S_{CH_3OH}). The X_{CO_2} values in the range of 433–473 K rise from 0.3% to 3.2%, while the S_{CH_3OH} decreases 100–63%. Moreover, though data in Table 3 indicate that the 80ZCZ catalyst ensures the maximum methanol yield, such a parameter cannot be directly related neither to SA nor to MSA values [22]. Indeed, the catalytic pattern of the studied system depicts some general trends irrespective of composition that disclose a marked negative influence of CO_2 conversion on methanol selectivity (Fig. 4A) and a straight increase in methanol productivity (STY) with temperature (Fig. 4B).

3.4. Surface sites and catalytic functionality

Even if the above findings do not rule out that some CO_2 adsorption/activation could also occur on metal copper [29,30], it has been documented that several surface sites of Cu, ZnO and ZrO_2 phases contribute to the adsorption–activation of H_2, CO and CO_2 on Cu/ZrO_2 and Cu–ZnO/ZrO_2 catalysts. On the basis of earlier kinetic and mechanistic findings showing that the CO_2 hydrogenation to methanol occurs with a very slow rate also at the surface of Cu single crystal [23,29,30], it can be inferred that both support and promoter somewhat enhance the functionality of Cu catalysts [22,23]. This points to the fundamental role of the metal/oxides interface on the methanol synthesis functionality of Cu [17,22]. In particular, the above results are consistent with the promoting effect of both ZrO_2 and ZnO on the CO_2 adsorption, markedly enhancing the surface

Table 3
Conversion-selectivity data ($X_{CO_2} - S_{CH_3OH}$) of Cu–ZnO/ZrO_2 catalysts in the CO_2 hydrogenation reaction at different temperature. (P_R, 1.0 MPa; GHSV, 8.8 NL h^{-1} g_{cat}^{-1}) and kinetic data of the CO_2 hydrogenation to methanol on Cu–ZnO/ZrO_2 catalysts at 473 K.

Catalyst	P_R, 1.0 MPa			Reaction rate[a]		E_a (kJ mol^{-1})
	T_R, 433 K	T_R, 453 K	T_R, 473 K	(μmol_{CH_3OH} $g_{cat^{-1}}$ s^{-1})	(μmol_{CH_3OH} $m_{cat^{-2}}$ s^{-1})	
CZ	0.6–100	1.2–85.5	2.2–83.0	5.02E−01	4.3E−03	57 ± 1
10ZCZ	0.5–100	1.1–86.6	2.1–71.5	4.83E−01	3.8E−03	58 ± 1
40ZCZ	0.6–100	1.4–83.8	2.9–64.7	5.14E−01	3.0E−03	69 ± 3
80ZCZ	0.7–100	1.5–83.3	3.2–64.7	5.62E−01	3.5E−03	66 ± 1
280ZCZ	0.3–100	0.9–85.9	2.1–63.3	3.85E−01	2.6E−03	78 ± 3

[a] Values taken from (Refs.' [22,23]).

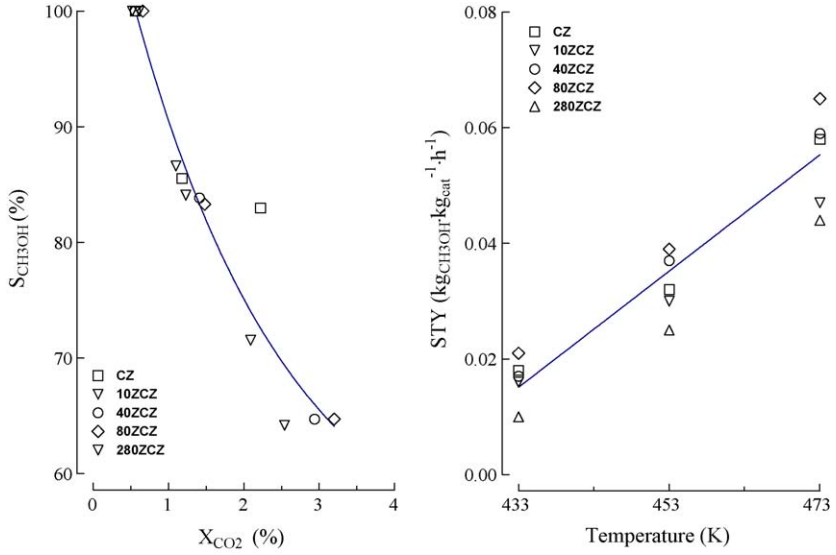

Fig. 4. (A) Methanol selectivity vs. CO_2 conversion and (B) STY of the various catalysts in the range 433–473 K at 1.0 MPa (GHSV, 8800 NL h^{-1} kg_{cat}^{-1}).

availability of the formate intermediate [23,29,30]. This explains the superior CO_2 hydrogenation functionality of Cu–ZnO/ZrO_2 catalysts in comparison to Cu/ZnO and Cu/ZrO_2 systems [17,22]. Further, kinetic data in Table 3 show that CZ and 10ZCZ catalysts feature lower apparent energy values (E_{app}, 57–58 kJ/mol) than catalysts with greater ZnO loadings (66–78 kJ/mol), characterised by increasing values of metal dispersion (Fig. 5). This substantiates the fact that the zirconia carrier enables an easier reactivity of the formate intermediate [13,14] in comparison to systems featuring a preferential Cu–ZnO interaction (e.g., $Zn_{at}/Cu_{at} > 0.1$). Then, the catalyst efficiency relies on a proper balance of hydrogenation and CO_2 activation sites in the neighbouring of the Cu-oxides interface, "borderline" for the formation and further hydrogenation of the *formate* intermediate [29,30]. The *dual-site* nature of the reaction pathway also would account for the "apparent" *structure-sensitive* character of the CO_2 hydrogenation reaction [22,23]. Namely, considering that both the $Cu^{\delta+}$-to-Cu^0 and oxide-to-metal surface area ([OSA/MSA] = [(SA − MSA)/MSA]) ratios are independent measures of the extent of the metal/oxides interface [23], the specific activity of the various catalysts normalized to the metal Cu (i.e., TOF) and $Cu^{\delta+}$ (TOF_1) site concentration and the oxide-to-metal surface area ratio (TOF_2) was calculated and plotted against the mean Cu particle size, as shown in Fig. 5. Although the TOF depicts an exponential-like decreasing trend, the last two parameters allow a thorough *normalization* of the catalytic activity, as both TOF_1 and TOF_2 result straight-line functions of metal dispersion (Fig. 5). Then, the reactivity pattern of the Cu–ZnO/ZrO_2 system ultimately points to factors, other than to MSA, like the critical parameters controlling the reactivity of the studied systems [22,23]. These findings match the evidence that the reactivity of Cu-promoted catalysts depends slightly upon the availability of surface hydrogen species, since this overwhelms that of the formate intermediate(s) [29]. Moreover, such results are consistent with the fact that the hydrogenation of the reactive intermediate on ZnO and ZrO_2 surface sites in the neighbouring of Cu centres is the *rate limiting step* (*r.l.s.*) of methanol synthesis reaction [18,23]. On the other hand, at variance of Cu^0 and surface basic sites of ZrO_2 and ZnO, very marginal seems the contribution of $Cu^{\delta+}$ centres in the main CO_2 hydrogenation path. Probably, the straight dependence of their concentration on the extent of the oxide/metal interface led to address their active role in methanol synthesis reactions [23].

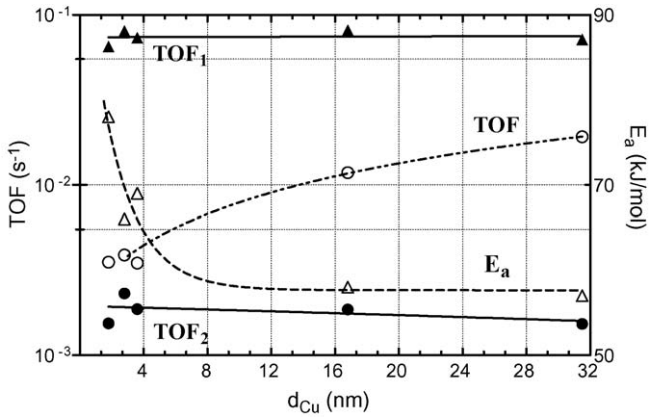

Fig. 5. Turnover frequency referred to Cu^0 (TOF) and $Cu^{\delta+}$ (TOF_1) site concentration and oxide-to-metal surface area ratio (TOF_2), and apparent activation energy (E_a) of methanol formation vs. the average Cu particle size (dCu). Experimental conditions: T_R, 473 K; P_R, 1.0 MPa; GHSV, 8800 NL h^{-1} kg_{cat}^{-1}.

4. Conclusions

The solid-state interaction pattern and the nature of surface adsorption sites of Cu–ZnO/ZrO_2 catalysts have been addressed, leading to the following main conclusions:

- A strong Cu–ZnO interaction effectively promotes the metal dispersion, determining also the redox properties and the reactivity of the Cu–ZnO/ZrO_2 system.
- The interaction of metal Cu particles with both ZnO and ZrO_2 leads to the stabilization of $Cu^{\delta+}$ sites at the metal/oxides interface.
- A "mixture" of Cu^0, $Cu^{\delta+}$ and Lewis basic sites concur to the adsorption–activation of H_2, CO and CO_2 on Cu–ZnO/ZrO_2 catalysts.
- The oxide/metal interface plays a fundamental influence on the CO_2 hydrogenation functionality by enabling the hydrogenation of the formate intermediate on the basic sites of ZnO and ZrO_2 by neighbouring metal sites.
- Unpredictable changes in the extent of the oxide/metal interface, due to surface reconstruction, re-crystallization and phase-segregation phenomena account for the poor, if any, dependence of the methanol productivity on MSA.

References

[1] G.A. Olah, A. Goeppert, G.K. Surya Prakash, Beyond Oil and Gas: The Methanol Economy, WILEY-VCH Verlag GmbH & Co., KGaA, Weinheim, 2006.
[2] G.A. Olah, A. Goeppert, G.K. Surya Prakash, Catal. Lett. 93 (2004) 1.
[3] C. Song, Catal. Today 115 (2006) 2.
[4] I. Omae, Catal. Today 115 (2006) 33.
[5] R.H. Borgwardt, Ind. Eng. Chem. Res. 37 (1998) 3760.
[6] J.C.J. Bart, R.P.A. Sneeden, Catal. Today 2 (1987) 1.
[7] M. Bowker, R.A. Hadden, H. Houghton, J.N.K. Hyland, K.C. Waugh, J. Catal. 109 (1988) 263.
[8] J. Weigel, R.A. Koeppel, A. Baiker, A. Wokaun, Langmuir 12 (1996) 5319.
[9] K.C. Waugh, Catal. Today 15 (1992) 51.
[10] A.T. Aguayo, J. Ereña, D. Mier, J.M. Arandes, M. Olazar, J. Bilbao, Ind. Eng. Chem. Res. 46 (2007) 5522.
[11] J. Ereña, R. Garoña, J.M. Arandes, A.T. Aguayo, J. Bilbao, Catal. Today 107/108 (2005) 467.
[12] C. Schild, A. Wokaun, A. Baiker, J. Mol. Catal. 63 (1990) 243.
[13] Y. Sun, P.A. Sermon, J. Chem. Soc., Chem. Commun. 16 (1993) 1242.
[14] I.A. Fisher, A.T. Bell, J. Catal. 178 (1998) 153.
[15] I.A. Fisher, A.T. Bell, J. Catal. 172 (1997) 222.
[16] D. Bianchi, T. Chafik, M. Khalfallah, S.J. Teichner, Appl. Catal. A 112 (1994) 57.
[17] W. Hertl, Langmuir 5 (1989) 96.
[18] S.E. Collins, D.L. Chiavassa, A.L. Bonivardi, M.A. Baltanás, Catal. Lett. 103 (2005) 83.
[19] C. Li, K. Domen, T. Onishi, J. Am. Chem. Soc. 111 (1989) 7683.
[20] M. Lachowska, J. Skrzypek, React. Kinet. Catal. Lett. 83 (2004) 269.
[21] J. Toyir, P.R. de la Piscina, J. Llorca, J.L.G. Fierro, N. Homs, Phys. Chem. Chem. Phys. 3 (2001) 4837.
[22] F. Arena, K. Barbera, G. Italiano, G. Bonura, L. Spadaro, F. Frusteri, J. Catal. 249 (2007) 183.
[23] F. Arena, G. Italiano, K. Barbera, S. Bordiga, G. Bonura, L. Spadaro, F. Frusteri, Appl. Catal. A Gen. 350 (2008) 16.
[24] P.L. Hansen, J.B. Wagner, S. Helveg, J.R. Rostrup-Nielsen, B.S. Clausen, H. Topsøe, Science 295 (2002) 2053.
[25] X.M. Liu, G.Q. Lu, Z.-F. Yan, J. Beltramini, Ind. Eng. Chem. Res. 42 (2003) 6518.
[26] P.R. Dennison, K.J. Packer, M.S. Spencer, J. Chem. Soc., Faraday Trans. 85 (1989) 3537.
[27] H. Wilmer, M. Kurtz, K.V. Klementiev, O.P. Tkachenko, W. Grünert, O. Hinrichsen, A. Birkner, S. Rabe, K. Merz, M. Driess, C. Wöll, M. Muhler, Phys. Chem. Chem. Phys. 5 (2003) 4736.
[28] J.D. Grunwaldt, C. Kiener, F. Schüth, A. Baiker, Phys. Scr. T115 (2005) 819.
[29] I. Chorkendorff, J.W. Niemantsverdriet, Concepts of Modern Catalysis and Kinetics, WILEY-VCH GmbH & Co., KGaA, Weinheim, 2005.
[30] P.B. Rasmussen, P.M. Holmblad, T. Askgaard, C.V. Ovesen, P. Soltze, J.K. Nørskov, I. Chorkendorff, Catal. Lett. 26 (1994) 373.